Magnetic-Field-Induced Ferroelectric Polarization Reversal in the Multiferroic $Ge_{1-x}Mn_xTe$ Semiconductor

H. Przybylińska,[1,*] G. Springholz,[2,†] R. T. Lechner,[2,3] M. Hassan,[2,4] M. Wegscheider,[2] W. Jantsch,[2] and G. Bauer[2]

[1]*Institute of Physics, Polish Academy of Sciences, Al. Lotników 32/46, 02-668 Warsaw, Poland*
[2]*Institut für Halbleiter-und Festkörperphysik, Johannes Kepler Universität, A-4040 Linz, Austria*
[3]*Institut für Physik, Montanuniversität Leoben, A-8700 Leoben, Austria*
[4]*Department of Physics, University of the Punjab, Lahore-54590, Pakistan*

(Received 25 March 2013; revised manuscript received 14 November 2013; published 29 January 2014)

$Ge_{1-x}Mn_xTe$ is shown to be a multiferroic semiconductor, exhibiting both ferromagnetic and ferroelectric properties. By ferromagnetic resonance we demonstrate that both types of order are coupled to each other. As a result, magnetic-field-induced ferroelectric polarization reversal is achieved. Switching of the spontaneous electric dipole moment is monitored by changes in the magnetocrystalline anisotropy. This also reveals that the ferroelectric polarization reversal is accompanied by a reorientation of the hard and easy magnetization axes. By tuning the GeMnTe composition, the interplay between ferromagnetism and ferroelectricity can be controlled.

DOI: 10.1103/PhysRevLett.112.047202 PACS numbers: 75.50.Pp, 75.30.Gw, 76.50.+g, 75.85.+t

Ferromagnetism in semiconductors has received much attention, both for its fundamental importance as well as for possible spintronic applications [1–3]. In the prototype $Ga_{1-x}Mn_xAs$ system [4], carrier mediated ferromagnetism (FM) is well understood and by control of the carrier density using electric fields, manipulation of the magnetization can be achieved [5]. Combination of $Ga_{1-x}Mn_xAs$ with ferroelectric (FE) gates [6] even allows persistent modulation of the magnetic properties by poling the gate material. Further effects are expected when combining ferroelectric and ferromagnetic ordering in one and the same material [7–13]. Such *multiferroics* have triggered immense interest because of their unique properties and potential device applications [14–16]. Single phase materials that show simultaneously ferroelectricity and ferromagnetism are, however, very rare [7–11]. This is due to a fundamental conflict: a cation can move off center in a crystal as a prerequisite for ferroelectricity if it has an empty d shell [17], whereas ferromagnetism of transition metal compounds requires cations with partly filled d shells. As shown in this work, this apparent contradiction can be lifted in $Ge_{1-x}Mn_xTe$, where the Ge^{2+} ions ($3d^0$) are responsible for ferroelectricity and the Mn^{2+} ions ($3d^5$) provide the magnetic moments for ferromagnetism mediated by free holes. Thus, GeMnTe offers unique semiconducting and multiferroic properties.

The host material GeTe is a narrow gap semiconductor and one of the simplest ferroelectrics consisting of only two atoms per primitive unit cell [18]. It undergoes a spontaneous paraelectric to ferroelectric phase transition at a Curie temperature $T_c^{FE} \sim 625$ K [18–20], below which the $Fm3m$ symmetry of the cubic rock salt structure is broken and a polar rhombohedral $R3m$ lattice is formed by elongation of the unit cell along a ⟨111⟩ direction [see Fig. 1(a)]. Because of the resulting relative displacement of the Ge and Te sublattices by about 0.35 Å along this distortion direction [18–20], a spontaneous FE polarization appears that persists even in small nanocrystals [19]. Because of native Ge vacancies, GeTe is naturally conducting with free hole densities in excess of 10^{20} cm^{-3} [21,22]. This results in strong internal screening of the spontaneous polarization. Nevertheless, its switching by electrical fields has been recently demonstrated by piezoresponse force microscopy [23]. The high hole density promotes ferromagnetic ordering when GeTe is doped with transition metal ions such as Cr [24], Fe [25], or Mn [26–31]. The solubility of Mn in GeMnTe is particularly high, reaching ~50% without impairing the crystalline quality [28,29,32]. As a result, FM transition temperatures T_C^{FM} above 150 K have been obtained [27–29], which is amongst the highest of all diluted FM semiconductors [2,3].

In this Letter, we present direct evidence for the coexistence and coupling between ferroelectricity and ferromagnetism in $Ge_{1-x}Mn_xTe$, thus demonstrating multiferroicity in this material system. By ferromagnetic resonance (FMR) we determine not only the magnetic properties but also the local site symmetry of magnetic ions [33–35] and, hence, the direction of the local FE dipole moment. As a result, simultaneous information on the FM and FE properties is obtained. Quantitative analysis of the FMR spectra shows that the magnetic anisotropy changes with FE lattice distortion and Mn content. Moreover, by varying the magnetic field direction we demonstrate magnetic-field-induced switching of the FE polarization and thus, coupling between the magnetic and electric dipole moments. This switching already occurs at low magnetic fields, which opens new incentives for device applications.

Epitaxial $Ge_{1-x}Mn_xTe$ layers were grown by molecular beam epitaxy on (111) BaF_2 substrates [28,29]. The layer thickness was set to 500 nm and the Mn content x_{Mn} varied from zero to 0.5 as determined by flux calibrations and secondary ion mass spectroscopy. The hole density of

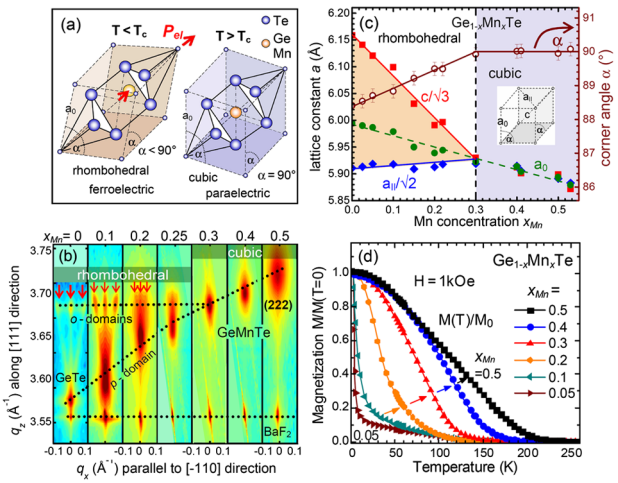

FIG. 1 (color online). (a) Primitive unit cell of $Ge_{1-x}Mn_xTe$ in the rhombohedral ferroelectric (left) and the cubic paraelectric phase (right). In the ferroelectric phase, the Ge(Mn) and Te sublattices are shifted with respect to each other along [111], producing an electric polarization $\boldsymbol{P}_{\rm el}$ as indicated by the arrow. (b) Reciprocal space maps around the (222) Bragg peak for $Ge_{1-x}Mn_xTe$ epilayers on BaF_2 (111) with $x_{\rm Mn}$ ranging from 0 to 0.5. For $x_{\rm Mn} < 0.3$, apart from the main peak due to p domains with FE polarization perpendicular to the surface, three secondary peaks (arrows) appear from o domains with $\boldsymbol{P}_{\rm el}$ along the oblique $\langle\bar{1}11\rangle$ directions. (c) Phase diagram of $Ge_{1-x}Mn_xTe$ at 300 K, showing the lattice parameters $a_\parallel/\sqrt{2}$ (diamonds), $c/\sqrt{3}$ (squares), and a_0 (dots) as well as the unit cell corner angle α (circles) as indicated in the inset. (d) Temperature dependent magnetization $M(T)/M(0)$ measured by SQUID in an external field of 1 kOe applied in plane.

$\sim 10^{21}$ cm^{-3} was controlled by excess Te flux. The substrate temperature was 310 °C which provides the highest structural perfection without secondary phases. High resolution x-ray diffraction (XRD) reciprocal space mapping was employed to determine the lattice structure. The magnetic properties were derived by SQUID magnetometry. FMR experiments were performed at 9.5 GHz using a Bruker ESR spectrometer using a TE102 cavity.

Figure 1(b) shows the (222) x-ray diffraction reciprocal space maps of $Ge_{1-x}Mn_xTe$ epilayers with varying Mn content. For $x_{\rm Mn} < 0.3$, besides the main Bragg peak from FE domains with rhombohedral distortion along the [111] surface normal direction ("p" domains), three secondary peaks appear (arrows), which arise from "o" domains with their distortion axes along one of the three oblique $\langle\bar{1}11\rangle$ directions. While in bulk GeTe all domains are equally abundant, in epilayers a preferential distortion along the growth direction, i.e., a strong preference for p-domain formation occurs. Accordingly, the diffracted intensity is about 20 times stronger than from the o domains [cf. Fig. 1(b)]. With increasing Mn content, the splitting of the domain peaks decreases and at $x_{\rm Mn} = 0.3$ all peaks merge into one, marking the rhombohedral-cubic transition at 300 K. Thus, for $x_{\rm Mn} < 0.3$ the ferroelectric transition is above room temperature.

From reciprocal space maps recorded around the asymmetric (153) Bragg reflection (see the Supplemental Material [36]), the in- and out-of-plane lattice parameters $a_\parallel$ and c were derived. The results are presented in Fig. 1(c) as a function of Mn content, together with the corresponding unit cell corner angles α (circles) and rhombohedral or cubic lattice constants a_0 (triangles) calculated using $\sin(\alpha/2) = a_\parallel/2a_0$ and $3a_0 = \sqrt{c^2 + 3a_\parallel^2}$. For GeTe, the measured corner angle $\alpha = 88.41°$ and lattice constant are in excellent agreement with recently reported values [19]. With increasing Mn content, a_0 linearly decreases as $da_0/dx = 0.123$ Å and the difference between $c/\sqrt{3}$ and $a_\parallel/\sqrt{2}$ vanishes for $x_{\rm Mn} = 0.3$, above which the cubic structure is formed. Thus, Mn incorporation reduces the tendency for rhombohedral lattice distortion, reducing the FE transition temperature to 300 K for $x_{\rm Mn} = 0.3$. Extrapolation of this trend gives a $T_c^{\rm FE} \sim 100$ K for $x_{\rm Mn} = 0.5$, indicating that ferroelectricity persists even up to high Mn concentrations.

All investigated $Ge_{1-x}Mn_xTe$ layers are single phase and ferromagnetic, as demonstrated by the magnetization $M(T)$ curves presented in Fig. 1(d). The FM Curie temperature $T_C^{\rm FM}$ strongly increases with increasing Mn content, approaching nearly 200 K for $x_{\rm Mn} = 0.5$. In addition, hysteresis loops recorded with magnetic field H applied parallel (along $\langle\bar{1}10\rangle$) or perpendicular to the layers reveal that with decreasing lattice distortion (i.e., increasing $x_{\rm Mn}$) a reorientation of the easy magnetization axis from the normal towards the in-plane direction occurs. This is shown for $x_{\rm Mn} = 0.2$ and 0.5 by Figs. 2(a) and 2(b), where for $x_{\rm Mn} \leq 0.2$ the remanent magnetization is higher in the perpendicular than in the in-plane direction, i.e., $M_\perp(0) > M_\parallel(0)$, whereas for $x_{\rm Mn} = 0.5$ this relationship is reverted. Thus, the magnetic anisotropy can be tuned by the Mn content [36]. As previously noted [27–30], the saturation magnetization M_s per Mn^{2+} ion is less than $5\mu_B$ expected for the $^5S_{5/2}$ spin-only ground state of Mn^{2+}. This means that not all Mn ions are FM ordered due to additional antiferromagnetic coupling between randomly distributed nearest neighbor Mn ions [27,28] superimposed on the long range RKKY interaction. However, extended antiferromagnetic MnTe clusters appear only for Mn contents above $x_{\rm Mn} > 0.5$, as shown by our previous studies [28,29].

To determine the correlation between ferromagnetism and ferroelectricity, we performed angular dependent FMR investigations to assess the local site symmetry of the Mn^{2+} cations and distinguish between different configurations of neighboring Te anions to detect the occurrence of a FE dipole moment. The uniform mode FMR frequency ν is given by the double derivatives $F_{\theta\theta}$, $F_{\varphi\varphi}$, and $F_{\theta\varphi}$ of the magnetic free-energy density F with respect to the polar and azimuthal angles θ and φ of the magnetization vector $\mathbf{M}$ relative to the crystal axes according to the Smit-Suhl equation [37,38]:

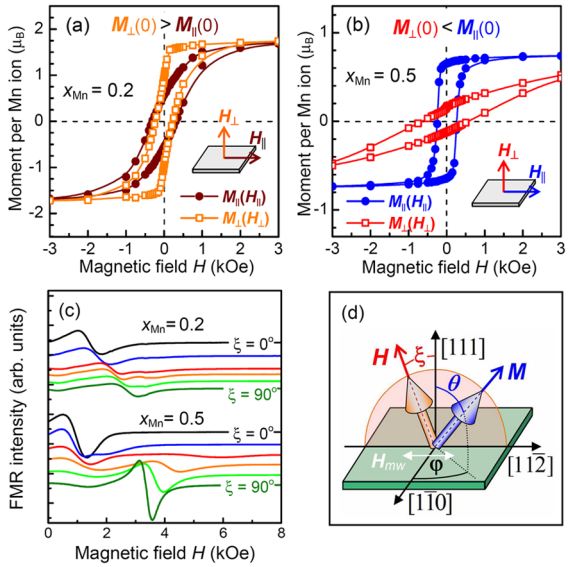

FIG. 2 (color online). Hysteresis curves $M(H)$ of $Ge_{1-x}Mn_xTe$ layers with x_{Mn} = (a) 0.2 and (b) 0.5. Open symbols: out-of-plane magnetic moment $M_\perp$ for H perpendicular to the layer, full symbols: in-plane magnetic moment $M_\parallel$ for H parallel to [$\bar{1}$01] as indicated by the insets. (c) FMR spectra for x_{Mn} = 0.2 and 0.5 for selected angles $\xi = 0°$, 30°, 60°, 70°, and 90° of the applied dc field H to the [111] surface. (d) Schematic illustration of the FMR geometry.

$$h\nu = \frac{g\mu_B}{M\sin\theta_{eq}}\sqrt{F_{\theta\theta}F_{\phi\phi} - F_{\theta\phi}^2}\Big|_{\theta_{eq},\phi eq}. \quad (1)$$

In this relation, g is the Landé factor, h the Planck constant, μ_B the Bohr magneton, and θ_{eq} and φ_{eq} the equilibrium angles of $\mathbf{M}$, determined by minimizing F. The anisotropic part of F in an applied magnetic field consists of the Zeeman energy $-\mathbf{H}\cdot\mathbf{M}$, the thin layer shape anisotropy $2\pi M^2\cos^2\theta$ and the magnetocrystalline anisotropy (MAE) due to the given point symmetry. For the case of a rhombohedral lattice, the contributions of cubic symmetry (with energy density parameter K_4) and of uniaxial symmetry up to fourth order (K_2 and $K_{4\|}$) can be separated as [39]

$$F = -\mathbf{H}\cdot\mathbf{M} + 2\pi M^2\cos^2\theta + K_2\sin^2\theta + K_{4\|}\sin^4\theta - \frac{2}{3}K_4\left[\sin^2\theta - \frac{7}{8}\sin^4\theta - \frac{\sqrt{2}}{2}\sin^3\theta\cos\theta\sin(3\varphi)\right], \quad (2)$$

where θ and φ are defined with respect to [111] and [1$\bar{1}$0], respectively. In our experiments, the microwave field $\mathbf{H}_{mw}$ was applied in plane along [1$\bar{1}$0] and the static field $\mathbf{H}$ rotated within the (1$\bar{1}$0) plane as shown schematically in Fig. 2(d). Representative FMR spectra are displayed in Fig. 2(c) for x_{Mn} = 0.2 and 0.5 at 2 K for selected angles ξ of $\mathbf{H}$ with respect to [111].

Polar plots of the measured FMR resonance fields H_r as a function of ξ are presented in Fig. 3 for x_{Mn} = 0.03, 0.15, 0.2, and 0.5 (symbols). For x_{Mn} = 0.3 and 0.4 the results are shown in the Supplemental Material [36]. The FMR data were modeled using Eqs. (1) and (2) and

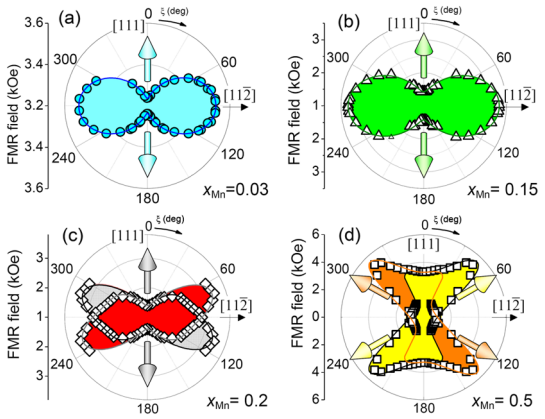

FIG. 3 (color online). Angular dependencies of the FMR positions at 2 K for x_{Mn} = 0.03 (a), 0.15 (b), 0.2 (c), and 0.5 (d). Symbols show experimental data, solid lines are calculated using Eqs. (1) and (2) and parameters listed in Table I. The polar angle ξ is defined in Fig. 3(d). Arrows indicate the easy magnetization axes (minima in FMR field).

the parameters in Table I (solid lines in Fig. 3), giving excellent agreement with the experimental data. For higher x_{Mn}, the fits of the FMR fields required effective g factors larger than the Landé value of 1.978. The corresponding shift in H_r is attributed to stray fields originating from spins that are exchange coupled to antiferromagnetically ordered Mn^{2+} ions at low temperatures. As can be seen in Figs. 3(a) and 3(b), for $x_{Mn} \leq 0.15$ the angular dependencies of H_r are well described, assuming only a second order *uniaxial* MAE with positive energy density K_2 ($K_4 = K_{4\|} = 0$; see Table I). Accordingly, the easy magnetization direction is along the [111] surface normal and the minimum FMR field occurs at $\xi = 0°$. All directions in the basal plane correspond to hard axes (maxima of H_r) in agreement with the SQUID data. Starting from x_{Mn} = 0.2, fourth order cubic terms K_4 come into play, which tilt the hard magnetization axes out of the layer plane. The negative sign of K_4 is characteristic for octahedrally coordinated magnetic ions [35].

In the absence of a rhombohedral distortion and shape anisotropy, the easy magnetization axis would lie along any of the four ⟨111⟩ cubic body diagonals and the hard axes along ⟨100⟩. For x_{Mn} = 0.2, however, due to the

TABLE I. Saturation magnetization M_s, anisotropy fields K_i/M_s, and g factors of $Ge_{1-x}Mn_xTe$ used for modeling the FMR data of Fig. 3. The second order anisotropy field does not allow distinction between contributions of uniaxial and shape anisotropies. Therefore, K_2/M was calculated taking for M the saturation magnetization obtained by SQUID.

x_{Mn}	M_s (emu/cm^3)	M_s (μ_B/Mn^{2+})	K_2/M_s (Oe)	$K_{4\|}/M_s$ (Oe)	K_4/M_s (Oe)	g factor
0.03	10	1.86	162	0	0	1.978
0.15	36	1.36	823	0	0	2.585
0.20	60	1.70	780	130	−300	2.419
0.5	67	0.76	−580	140	−1150	2.605

rhombohedral lattice distortion the easy magnetization axis is still parallel to [111], whereas for $x_{\mathrm{Mn}} = 0.5$ it rotates towards the oblique $\langle 11\bar{1} \rangle$ directions as indicated by arrows in Figs. 3(c) and 3(d), respectively. As shown in Table I, this spin reorientation is induced by the change of sign of the second order anisotropy field from $K_2/M = 780$ kOe for $x_{\mathrm{Mn}} = 0.2$ to $K_2/M = -580$ kOe for $x_{\mathrm{Mn}} = 0.5$. A positive value of K_2 signifies a rhombohedron elongated along the surface normal direction ($c > \sqrt{3/2}a_{\parallel}$), whereas a negative sign indicates a contracted rhombohedron ($c < \sqrt{3/2}a_{\parallel}$) for the $x_{\mathrm{Mn}} = 0.5$ epilayer, where we expect a small tensile strain induced by cooling to cryogenic temperatures.

In the case of a centrosymmetric rhombohedral lattice distortion alone, only *one* FMR resonance would occur for any magnetic field direction. For $x_{\mathrm{Mn}} \geq 0.2$, however, we actually observe *two* resonances for various magnetic field orientations [see Figs. 2(c), 3(c), and 3(d)]. These arise from differently oriented FE and FM domains that share the out-of-plane [111] and in-plane [1$\bar{1}$0] axes but have an opposite relative displacement of the cation and anion sublattices, i.e., a FE polarization in opposite direction. This is clearly evidenced by the mirror symmetric angular dependencies of the FMR positions in Figs. 3(c) and 3(d). For $x_{\mathrm{Mn}} = 0.2$, one domain has the hard axis (maximum H_r) at $\xi = 110°$ and the other at $\xi = 70°$; i.e., both are rotated out of the plane towards the [001] direction. For $x_{\mathrm{Mn}} = 0.5$, the hard axes lie at $\xi = 43°$ and the other at $\xi = 137°$, whereas the easy axes lie at $\xi = 117°$ and $\xi = 63°$. Similar results are obtained for the samples with $x_{\mathrm{Mn}} = 0.3$ and 0.4 [36]. This observation of *two* domains, further on referred to as "*A*" and "*B*" domains, proofs that the structure is not only rhombohedral but also *acentric* as required for ferroelectricity. Hence, the layers possess a spontaneous dipole moment along the [111] directions, demonstrating that $Ge_{1-x}Mn_xTe$ is ferromagnetic *and* ferroelectric up to $x_{\mathrm{Mn}} = 0.5$. Indeed, GeMnTe with its Shubnikov symmetry of "class 3" belongs to the 13 Shubnikov point groups that allow simultaneous appearance of spontaneous electric polarization and magnetization [9,11] as is required for multiferroic materials. For $x_{\mathrm{Mn}} = 0.5$, the two resonances are observed up to temperatures of about 100 K close to the ferroelectric phase transition extrapolated from the x-ray data. Above only one single resonance remains (see the Supplemental Material [36]). This indicates that the two resonances are indeed of ferroelectric origin.

To demonstrate ferroelectric switching induced by external magnetic fields, we analyze the relative domain volumes given by their integrated FMR intensities. Figure 4(a) shows the Lorentzian-shaped microwave absorption of the *A* (grey) and *B* (red) domains for $x_{\mathrm{Mn}} = 0.2$ at different angles ξ between **H** and [111] extracted from the FMR spectra. For $\xi < 90°$, the peaks from the *A* domains are much more intense than those of the *B* domains, whereas for $\xi > 90°$ the intensity ratio is almost exactly reversed. This clearly shows that FE domains can be manipulated by the applied magnetic field. The switching of the domains is quantified by plotting in Fig. 4(b) the FMR intensity ratios $I_{A(B)}/(I_A + I_B)$ as a function of magnetic field strength $H_{rz} = H_r \cos\xi$ along the [111] direction for the *A* (grey) and *B* (red) domains, respectively. The same procedure is applied for $x_{\mathrm{Mn}} = 0.5$ with the results depicted in Fig. 4(c). For both cases, a very abrupt intensity reversal occurs upon reversing the magnetic field direction, meaning that the electric polarization is switched from the [111] to the [$\bar{1}\,\bar{1}\,\bar{1}$] direction, as shown by the insets in Fig. 4. Remarkably, the switching is nearly complete, involving about 80% of the domain volumes at switching fields $|H_z|$ below 500 Oe. Moreover, for $x_{\mathrm{Mn}} = 0.5$ this switching is observed up to temperatures of 80 K close to the ferroelectric Curie temperature [36].

The switching of the electric dipole by the magnetic field is clear evidence for magnetoelectric coupling between ferromagnetism and ferroelectricity in GeMnTe, which is a characteristic feature of multiferroic materials [7–12] where the magnetic and electric susceptibility that limit its strength can become large at the same time [7–9]. Most notably, in GeMnTe the reversal of the FE moment already occurs at magnetic fields much lower than in most other single phase multiferroics [9,12], which often show only weak magnetic or weak ferroelectric order (i.e., susceptibilities) or both. Comparably small switching fields have been only reported for hexaferrite multiferroics [40] that exhibit, however, a complex helimagnetic spin structure. Since GeMnTe represents a multiferroic system with RKKY type ferromagnetism, its modeling by magnetoelectric coupling theories may provide new insights into the microscopic origin of this effect.

To conclude, we have demonstrated multiferroic behavior of GeMnTe, representing the structurally simplest multiferroic material discovered to date. In this system,

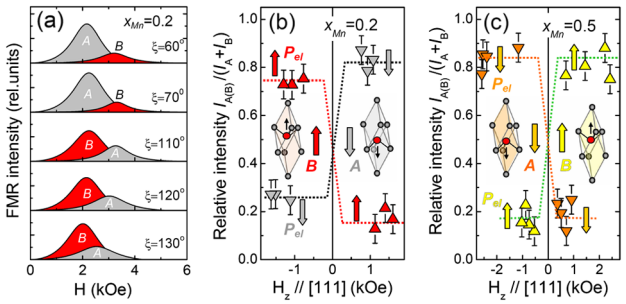

FIG. 4 (color online). (a) FMR absorption peaks derived for $Ge_{0.8}Mn_{0.2}Te$ from the fit of the spectra of Fig. 3(b) for different orientations ξ of the magnetic field. The intensity ratios $I_{A(B)}/(I_A + I_B)$ of the *A* (upward triangle) and *B* (downward triangle) domains are plotted in (b) and (c) for $x_{\mathrm{Mn}} = 0.2$ and 0.5, respectively, as a function of H_z ($= H\cos\xi$) along [111]. Dotted lines are guides for the eye. The insets show the primitive cell of GeMnTe with the two possible relative cation or anion displacements along [111] or [$\bar{1}\,\bar{1}\,\bar{1}$]. The corresponding opposite direction of the electric dipole $\boldsymbol{P}_{\mathrm{el}}$ is indicated by arrows.

ferroelectricity is due to the lattice distortion caused by Ge^{2+} ions and ferromagnetism due to the spins of the Mn^{2+} ions. As a result, both types of orders can be sustained and their relative strengths tuned by the Ge/Mn concentration. Our FMR results show that ferromagnetism and ferroelectricity are coupled to each other and thereby switching of the FE polarization by external magnetic fields is achieved, accompanied by reorientation of the easy axes of magnetization. In contrast to other multiferroics, GeMnTe is a multiferroic semiconductor, in which the strength of the ferromagnetic interactions can be controlled by the carrier concentration [27]. This may provide new avenues for novel spintronic and magnetoelectronic materials and devices.

We thank X. Marti, A. Ney, V. Ney, R. Kirchschlager, and D. Kriegner for helpful discussions and the Austrian Science Fund (Projects P20550-N20 and P18942-N20), GMe and ÖAD, Vienna, the European Science Foundation (FoNE SPINTRA), and the European Commission Network SemiSpinNet (PITN-GA-2008-215368) for support.

*Corresponding author.
przyby@ifpan.edu.pl
†Corresponding author.
gunther.springholz@jku.at

[1] J. K. Furdyna and J. Kossut, *Diluted Magnetic Semiconductors*, Semiconductors and Semimetals Vol. 25 (Academic, New York, 1988).
[2] T. Dietl, Nat. Mater. **9**, 965 (2010); T. Dietl and H. Ohno, Rev. Mod. Phys., (to be published).
[3] T. Jungwirth, J. Sinova, J. M. J. Kučera, and A. H. MacDonald, Rev. Mod. Phys. **78**, 809 (2006).
[4] H. Ohno, Science **281**, 951 (1998).
[5] D. Chiba, M. Sawicki, Y. Nishitani, Y. Nakatani, F. Matsukura, and H. Ohno, Nature (London) **455**, 515 (2008).
[6] I. Stolichnov, S. W. E. Riester, H. J. Trodahl, N. Setter, A. W. Rushforth, K. W. Edmonds, R. P. Campion, C. T. Foxon, B. L. Gallagher, and T. Jungwirth, Nat. Mater. **7**, 464 (2008).
[7] J. W. Eerenstein, N. D. Mathur, and J. F. Scott, Nature (London) **442**, 759 (2006).
[8] H. Schmid, J. Phys. Condens. Matter **20**, 434201 (2008).
[9] K. F. Wang, J.-M. Liu, and Z. F. Ren, Adv. Phys. **58**, 321 (2009).
[10] D. Khomskii, Physics **2**, 20 (2009).
[11] R. Ramesh and N. A. Spaldin, Nat. Mater. **6**, 21 (2007).
[12] Y. Tokura and S. Seki, Adv. Mater. **22**, 1554 (2010).
[13] A. R. Akbashev and A. R. Kaul, Russ. Chem. Rev. **80**, 1159 (2011).
[14] M. Gajek, M. Bibes, S. Fusil, K. Bouzehouane, J. Fontcuberta, A. Barthélémy, and A. Fert, Nat. Mater. **6**, 296 (2007).
[15] E. Y. Tsymbal, A. Gruverman, V. Garcia, M. Bibes, and A. Barthélémy, MRS Bull. **37**, 138 (2012).
[16] Y. H. Chu *et al.*, Nat. Mater. **7**, 478 (2008).
[17] N. Hill, J. Phys. Chem. **104**, 6694 (2000).
[18] W. Jantsch, *Dielectric Properties and Soft Modes in Semiconducting (Pb, Sn, Ge)Te*, Springer Tracts in Modern Physics Vol. 99 (Springer Verlag, Berlin, 1983).
[19] M. J. Polking *et al.*, Nano Lett. **11**, 1147 (2011).
[20] D. Lencer, M. Salinga, B. Grabowski, T. Hickel, J. Neugebauer, and M. Wuttig, Nat. Mater. **7**, 972 (2008).
[21] R. Tsu, W. E. Howard, and L. Esaki, Phys. Rev. **172**, 779 (1968).
[22] R. Shaltaf, X. Gonze, M. Cardona, R. K. Kremer, and G. Siegle, Phys. Rev. B **79**, 075204 (2009).
[23] J. J. Gervacio-Arciniega, E. Prokhorov, F. J. Espinoza-Beltran, and G. Tapaga, J. Appl. Phys. **112**, 052018 (2012).
[24] Y. Fukuma, H. Asada, T. Taya, T. Irisa, and T. Koyanagi, Appl. Phys. Lett. **89**, 152506 (2006).
[25] F. Tong, J. H. Hao, Z. P. Chen, G. Y. Gao, and X. S. Miao, Appl. Phys. Lett. **99**, 081908 (2011).
[26] R. Cochrane, M. Plishke, and J. Ström-Olsen, Phys. Rev. B **9**, 3013 (1974).
[27] Y. Fukuma, H. Asada, S. Miyawaki, T. Koyanagi, S. Senba, K. Goto, and H. Sato, Appl. Phys. Lett. **93**, 252502 (2008).
[28] R. T. Lechner, G. Springholz, M. Hassan, H. Groiss, R. Kirchschlager, J. Stangl, N. Hrauda, and G. Bauer, Appl. Phys. Lett. **97**, 023101 (2010).
[29] M. Hassan, G. Springholz, R. T. Lechner, H. Groiss, R. Kirchschlager, and G. Bauer, J. Cryst. Growth **323**, 363 (2011).
[30] W. Q. Chen, S. T. Lim, C. H. Sim, J. F. Bi, K. L. Teo, T. Liew, and T. C. Chong, J. Appl. Phys. **104**, 063912 (2008).
[31] A. Ciucivara, B. R. Sahu, and L. Kleinman, Phys. Rev. B **75**, 241201(R) (2007).
[32] W. Johnston and D. Sestrich, J. Inorg. Nucl. Chem. **19**, 229 (1961).
[33] X. Liu, Y. Sasaki, and J. K. Furdyna, Phys. Rev. B **67**, 205204 (2003); Y. Y. Zhou, X. Liu, J. K. Furdyna, M. A. Scarpulla, and O. D. Dubon, Phys. Rev. B **80**, 224403 (2009).
[34] D. Ehlers, V. Tsurkan, H.-A. Krug von Nidda, and A. Loidl, Phys. Rev. B **86**, 174423 (2012).
[35] A. Abragam and B. Bleaney, *Electron Paramagnetic Resonance of Transition Ions* (Clarendon Press, Oxford, 1970).
[36] See Supplemental Material at http://link.aps.org/supplemental/10.1103/PhysRevLett.112.047202 for additional structural and magnetic data as well as for temperature dependent FMR measurements.
[37] J. Smit and H. G. Beljers, Philips Res. Rep. **10**, 113 (1955); H. Suhl, Phys. Rev. **97**, 555 (1955).
[38] M. Farle, Rep. Prog. Phys. **61**, 755 (1998).
[39] L. D. Landau, E. M. Lifshitz, and L. P. Pitaevski, *Electrodynamics of Continuous Media. Course of Theoretical Physics* (Elsevier, New York, 2004), 2nd ed., Vol. 8.
[40] S. Ishiwata, Y. Taguchi, H. Murakawa, Y. Onose, and Y. Tokura, Science **319**, 1643 (2008).